accepted by ApJ Jan 06 2000

Spectral Energy Distributions for Disk and Halo M–Dwarfs

S.K. Leggett
Joint Astronomy Centre, University Park, Hilo, HI 96720
skl@jach.hawaii.edu

F. Allard
CRAL, Ecole Normale Superieure, 46 Allee d'Italie, Lyon, 69364 France
fallard@cral.ens-lyon.fr

Conard Dahn
Naval Observatory Flagstaff Station, Flagstaff AZ 86002-1149
dahn@nofs.navy.mil

P.H. Hauschildt
Department of Physics and Astronomy & Center for Simulational Physics,
University of Georgia, Athens, GA 30602-2451
yeti@hal.physast.uga.edu

T.H. Kerr
Joint Astronomy Centre, University Park, Hilo, HI 96720
tkerr@jach.hawaii.edu

and

J. Rayner
IRTF, 2680 Woodlawn Drive, Honolulu HI 96822
rayner@irtf.ifa.hawaii.edu

ABSTRACT

We have obtained infrared (1—2.5μm) spectroscopy for 42 halo and disk dwarfs with spectral type M1 to M6.5. These data are compared to synthetic spectra generated by the latest model atmospheres of Allard & Hauschildt. Photospheric parameters metallicity, effective temperature and radius are determined for the sample.

We find good agreement between observation and theory except for known problems due to incomplete molecular data for metal hydrides and H_2O. The metal–poor M subdwarfs are well matched by the models as oxide opacity sources are less important in this case. The derived effective temperatures for the sample range from 3600 K to 2600 K; at these temperatures grain formation and extinction are not significant in the

photosphere. The derived metallicities range from solar to one-tenth solar. The radii and effective temperatures derived agree well with recent models of low mass stars.

The spectra are available in electronic form, on request.

1. Introduction

Until very recently the observational data for low–mass stars could not be well reproduced by synthetic spectra or photometry. The cool, high–pressure atmospheres are difficult to model, due in particular to complex opacity sources: strong molecular bands and, for the halo stars and very low–mass objects, pressure–induced molecular hydrogen opacity (see e.g. Borysow, Jørgensen & Zheng 1997). The situation is now much improved as demonstrated by for example the "NextGen" models of Hauschildt, Allard & Baron 1999 (see also Allard et al. 1997). The observational side of the study of low–mass stars has also changed remarkably with a large increase in the known number of low–mass stars, brown dwarfs, and even giant planets.

For the last several years we have been obtaining infrared spectra for a sample of halo and disk stars approaching and even below the stellar/sub–stellar boundary. This work extends the similar spectroscopic study presented by Leggett et al. 1996 to more metal–poor and lower mass regimes, and builds on the photometric study published recently by us (Leggett et al. 1998). The spectra are compared to synthetic spectra generated from an improved version of Allard & Hauschildt's NextGen model atmospheres (Hauschildt, Allard & Baron 1999). In this paper we will present the results for the hotter stars in the sample, those with effective temperature higher than 2500 K, where neither grain condensation or extinction is significant. A subsequent paper will present our results for the cooler objects.

In §2 we describe the various instruments that have been used for this project. The target sample is described in §3 where we illustrate the likely range of metallicity and effective temperature through color–color and magnitude–color diagrams. §4 gives the observational results in the form of selected sets of spectra as well as integrated fluxes and bolometric magnitudes. §5 gives a brief description of the models and the comparison process. The results of the comparison of the data to the synthetic spectra are presented in §6 and our conclusions given in §7.

2. Instrumentation

We have been obtaining 1—2.5μm spectra of low mass stars for the last few years, where the targets have been selected to sample a broad range of temperature and metallicity. Here we present the results for forty-two of the stars, those with spectral type earlier than M7, and effective temperature hotter than 2500 K. The observing runs occurred in 1999 April, 1998 January, 1997 November and 1997 April using CGS4 at UKIRT on Mauna Kea, and 1994 July using KSPEC at the University of Hawaii's 88–inch telescope on Mauna Kea. KSPEC is a cross–dispersed

spectrometer with a 1024×1024 HgCdTe detector. CGS4 is a grating spectrometer with a 256×256 InSb detector. Fainter stars could be observed with CGS4 than with KSPEC, however KSPEC provided spectra from 0.9μm to 2.4μm in a single exposure, compared to the four grating settings required by CGS4.

For 9 of the stars we have obtained optical spectra using spectrometers in Hawaii in 1996 April, and in Flagstaff Arizona in 1989 December and 1989 September. In Arizona we used the B & C spectrograph on the 72–inch Lowell telescope and the spectrograph on the Naval Observatory Flagstaff Station's 40–inch telescope. In Hawaii we used the HARIS spectrograph at the UH 88–inch telescope.

Table 1 lists the observing dates, grating and slit information, and resolutions, provided by these instruments. In the cases where we did not have our own optical spectra we have obtained spectra from the literature. These sources are described below.

Data reduction was carried out in the usual way using the IRAF and Figaro software packages. For the infrared data, the effect of the terrestrial atmosphere was removed by dividing by the spectrum of a nearby early–type star, after removing hydrogen lines seen in this reference spectrum. The shape of the infrared spectrum is corrected for the known flux distribution of the early–type star. The spectral segments were individually flux calibrated using the targets known IJHK photometry. Each section was integrated over the appropriate filter profile (Cousins I or UKIRT JHK); the observed flux from Vega was integrated over the same profile. Vega was assumed to be zero magnitude at all wavelengths, and the target flux was scaled to match the broadband photometry. Where we obtained optical spectra from the literature these were flux calibrated by us in the same way (using either an R or I filter as appropriate).

3. The Sample

3.1. Sample Selection

Infrared spectra were obtained for a selection of the very low–mass stars of the halo and disk. The halo stars were selected from studies of known high proper–motion stars by Gizis 1997, Gizis & Reid 1997 and Monet et al. 1992. The disk stars are also known proper motion objects, and were selected from Leggett 1992 to sample metallicity and a range of effective temperature. The targets are listed in Table 2. We give LHS or LP number (Luyten 1979), and/or Gliese or Gliese/Jahreiss number (Gliese & Jahreiss 1991), and/or Giclas number (Giclas, Burnham & Thomas 1971), for each star. An abbreviated RA/Dec is also given to aid identification. Note that LHS 421 is the well–known eclipsing binary CM Draconis (also known as Gliese 630.1A, Metcalfe et al. 1966).

The spectral types in Table 2 are taken from various sources and there may be discrepancies or errors at the level of one sub–class. For the halo stars the classifications primarily are from Gizis 1997 and Gizis & Reid 1997, but for LHS 2045 and LHS 3390 they are based on our own

optical spectra. For the disk stars the classifications are taken from Gizis 1997, Kirkpatrick, Henry & Simons 1995 and Kirkpatrick, Henry & Irwin 1997.

The kinematic populations have been taken from Leggett et al. 1998, Leggett 1992. For a few objects the classifications of Leggett 1992 have been updated using radial velocities from Reid, Hawley & Gizis 1995 and Dawson & de Robertis 1998. The classification schemes for young disk (YD), young/old disk (Y/O), old disk (OD), old disk/halo (O/H) and halo (H) are described in Leggett 1992.

Table 2 also lists the instrumentation used for each object using the configuration names given in Table 1. Where we did not have our own optical data available we used published spectra taken from the sources listed in the Table. The instrumental resolutions for these data are given in the notes to the Table.

3.2. Photometrically Implied Properties of the Sample

Table 3 lists distance moduli and VIJHKL′ colors for the sample, taken primarily from the compilations by Leggett 1992, Leggett et al. 1998 — the reader is asked to refer to these papers for the data sources. V,I for LHS 425 are unpublished Naval Observatory Flagstaff Station data. New L′ data have been obtained by us for LHS 1174, LHS 523 and LHS 5328 in 1999 September using the reconfigured IRCAM/TUFTI camera on UKIRT at Mauna Kea. These data are presented in Table 3. As shown by Leggett et al. 1998 the NextGen models (Hauschildt, Allard & Baron 1999) do a very good job of reproducing the observed photometry. The most recent models include a new linelist for TiO (Schwenke 1998) which has improved the match to the energy distribution in the optical to red regime (compare our Figure 1 to Figure 1 of Leggett et al. 1998). The new models also include a new linelist for H_2O (Partridge & Schwenke 1997) however the calculated and observed water band strengths still show some discrepancies. This is discussed further below.

Figures 1 to 4 show VIJHKL′ color–color diagrams with model synthetic color sequences overlaid. The most metal-poor stars and coolest stars are identified. Figure 5 shows M_J:J−K with isochrones from the structural models by Baraffe et al. 1997, Chabrier & Baraffe 1997. These use the NextGen atmospheres but not the most recent versions with the improved linelists. Nevertheless the agreement is good and we can estimate mass and metallicities for our objects from this diagram. Note that the empirical masses based on the Henry & McCarthy 1993 scale (shown on the right axis) agree well with these structural models. The more recent mass–luminosity paper by Henry et al. 1999 supports their previous work.

Figures 1 through 5 imply that our sample covers a range of metallicity of about solar to about 3% of solar (m/H~ -1.5) and the range in effective temperature is about 3800 K to 2400 K. The implied mass range is 0.3—0.1$M/M_\odot$ for the halo stars, 0.6—0.09$M/M_\odot$ for the disk stars. A grid of synthetic spectra were calculated covering this range of likely values, and more exact determinations of effective temperature and metallicity are presented later as a result of

comparison to the synthetic spectra.

4. Observational Results

4.1. Spectroscopic Sequences

Figure 6 shows a representative set of spectra for approximately solar metallicity objects with a range of effective temperature and spectral type. The obvious features to note, which strengthen with decreasing temperature, are: the CO bands at 2.3μm; the water bands at around 1.4μm, 1.8μm and 2.4μm; the FeH band at 0.99μm; and the KI doublets at around 1.18μm and 1.24μm. A more complete list of spectral features seen in the M–dwarfs is given in Leggett et al. 1996.

Figure 7 demonstrates the effect of metallicity at $T_{eff} \sim 3000$ K. The shape of the infrared energy distribution for the metal–poor stars becomes dominated by pressure–induced H_2 opacity. There are no strong absorption features seen in the subdwarfs in the infrared, but in the optical the hydride features are a good indicator of a subdwarf nature — the hydride features, especially CaH at 0.69μm, become very strong relative to the TiO bands.

4.2. Integrated Fluxes and Bolometric Corrections

Table 3 gives integrated fluxes for the sample, expressed as flux at the Earth, bolometric magnitude and intrinsic stellar luminosity. The integrated fluxes were obtained by integrating our spectroscopic data over wavelength, and adding the flux contributions at shorter and longer wavelengths. Some stars had gaps in our spectroscopic data around 1μm. The contributions from these regions were estimated using stars of similar spectral type with complete spectral coverage.

The flux contributions at wavelengths beyond 2.4μm were calculated by deriving the flux at L$'$ using an effective wavelength approach, summing the contribution from the end of the K–band spectrum to this point with a linear interpolation, and assuming a Rayleigh–Jeans tail beyond L$'$. Theoretical energy distributions imply that the error in a Rayleigh–Jeans assumption is $\ll$1% for this sample. For stars without L$'$ photometry, L$'$ was estimated from stars of similar J$-$K color and metallicity.

Most of our stars have spectra available starting around 0.6μm. For these stars the shorter wavelength flux contribution was adopted to be a simple linear extrapolation to zero flux at zero wavelength from the flux at 0.6μm, except for the hottest stars where the flux at B was estimated using the effective wavelength approach, and linear interpolations used from zero wavelength to B, and from B to the start of the red spectrum. For the two stars without optical spectra the contribution in this region was estimated from stars of similar temperature and metallicity. For the hotter of these two stars, LHS 5327, there is a relatively large uncertainty in the total flux

due to the lack of optical data; for this star the uncertainty in total flux is 10%, leading to an uncertainty of 0.10mag in the bolometric correction and 0.05dex in $\log_{10} L/L_{\odot}$. For the rest of our sample the uncertainties are 5%, 0.05 mag and 0.02dex, respectively.

Figure 8 plots K–band bolometric correction against I−K color. We have included the results from Leggett et al. 1996. The approximate metallicities of the stars are indicated, based on kinematic population. Model sequences are overlaid as dashed lines, where again these model calculations have not been upgraded to include the new TiO or H_2O linelists but still match the observations well. The metal–poor stars are confined to small values of BC_K due to the onset of pressure–induced H_2 opacity, reducing the flux at K. For the disk stars the relationship between K–band bolometric correction and I−K color can be well represented by the cubic polynomial:

$$BC_K = -2.741 + 5.452(I-K) - 1.824(I-K)^2 + 0.211(I-K)^3$$

for $1.8 \leq$ I−K ≤ 3.3. This fit is indicated by the solid line in Figure 8.

5. Models and Synthetic Spectra, and Comparison Process

We have calculated the models presented in this paper using our multipurpose model atmosphere code Phoenix, version 10.7. Details of the code and the general input physics setup are discussed in the description of the NextGen grid of model atmospheres presented by Hauschildt, Allard & Baron 1999 and references therein. The model atmospheres presented here were calculated with the same general input physics as the NextGen models. However, a change of the linelists has significant impact on the model structure and synthetic spectra. The most important difference from our NextGen grid is the replacement of TiO and H_2O linelists with the newer linelist calculated by the NASA–AMES group, Schwenke 1998 for TiO (about 175 million lines of 5 isotopes) and Partridge & Schwenke 1997 for H_2O (about 350 million lines in 2 isotopes). Our combined molecular line list includes about 550 million molecular lines. These lines are treated with a direct opacity sampling technique where each line has its individual Voigt (for strong lines) or Gauss (weak lines) line profile, see Hauschildt, Allard & Baron 1999 and references therein for details. The number of lines selected by this procedure depends on the the model parameters. In addition to the new line data, we have also included dust formation and opacities in the models used in this paper. However, the lowest effective temperatures of the stars we consider here are slightly above the regime were dust formation and opacities are important. A complete description of the models and the differences to the NextGen models will be given in Allard & Hauschildt (1999, in preparation).

The fitting of the synthetic to the observed spectra was done using an automatic IDL program. First, the resolution of the synthetic spectra is reduced to that of each individual observed spectrum and the spectra are normalized to unit area for scaling. The comparison was done using a model atmosphere grid that covers the range 1500 K$\leq$ $T_{eff} \leq$ 4000 K, $3.5 \leq \log g \leq 5.5$ and $-1.5 \leq$ [m/H] ≤ 0.0, with a total of 221 model atmospheres. For each observed spectrum

we then calculate the χ^2 value for the comparison with all synthetic spectra in the grid. In order to avoid known problematic spots in either the observations or the synthetic spectra, the wavelength ranges 1.35—1.5μm and 1.8—1.95μm were excluded from the comparison, however, tests showed this did not significantly change the results. We selected the models that resulted in the lowest 3—5 χ^2 values as the most probable parameter range for each individual star. The "best" value was then chosen by visual inspection. This procedure allows a rough estimate of the probable range in the stellar parameters. Note that systematic errors due to missing or incomplete opacity sources are not eliminated, however investigations of the different linelists available for TiO and H_2O indicate that differences in the treatment of these opacity sources effect the implied effective temperatures in opposite senses (Allard, Hauschildt & Schwenke 2000) — i.e. the systematic errors should be small.

6. Results of Comparison of Data and Models

The automatic comparison described in the previous section resulted in χ^2 values between 0.02 and 0.10, with an average value of 0.05. The best fits were inspected by eye and in some cases a match with a slightly higher χ^2 value than minimum was adopted. We did not try to match the bottom of the water bands, but did look at the depth of the CO and TiO bands, and tried to match the overall "continuum" in the optical and infrared regimes. For the metal–poor stars the flatness of the infrared continuum could be used to constrain the derived metallicities.

Based on visual inspection and the χ^2 values, the uncertainty in the derived values of effective temperature is $\pm$100 K, and in metallicity ([m/H]) $\pm$0.25 dex. Gravity could not be well constrained by data of this relatively low resolution — spectra generated with log g values of 5.0 $\pm$0.5 dex all matched the data well. Table 4 lists the derived parameters for the sample. For the two stars in common with Leggett et al. 1996 who used earlier NextGen atmospheres, the agreement is within the quoted 150 K errors for that work (for LHS 57 the temperature derived here is identical and for LHS 377 it is 150 K cooler).

Figure 9 shows comparisons of synthetic and observed spectral energy distributions for approximately solar-metallicity stars with effective temperatures of 3600 K (LHS 65), 3100 K (LHS 421) and 2600 K (LHS 523). Also shown is a more metal–poor star with T_{eff} =3200 K (LHS 3061). The fits are good except for the coolest temperatures where problems with the water opacity became apparent, and where details of grain formation and settling may become important. The strength of the FeH line at 1μm is also overestimated in the models. These new models have resolved the discrepancy between the infrared and optical regions seen by Viti et al. 1997 for the eclipsing binary CM Draconis (LHS 421); Figure 9 shows that the entire energy distribution is well matched by a model with T_{eff} =3100 K and [m/H]= -0.5.

Figures 10—12 show derived T_{eff} as a function of various colors. Symbols indicate the metallicity implied by the energy distribution comparison (given in Table 4) — metal–poor

stars are bluer at a constant temperature, except in V−I at $T_{eff} \leq 2900$ K. The solid lines are model–predicted temperature:color relationships; the apparent offset for the infrared colors of the disk stars is probably due to the remaining problems with water opacity, which is more significant at cooler temperatures. The error in color due to absolute calibration or observational error is smaller than the apparent offset. We note that the observed trend of T_{eff} with V−I and I−K colors agrees with that implied by our earlier work using the NextGen atmospheres (Leggett et al. 1996, Figure 17) but the agreement between observation and theory for V−I is much improved with the new TiO linelist.

Diameters have been derived for the stars in the sample in two ways. One was to use the scaling factors necessary to match the synthetic stellar surface spectra to that observed at the Earth, which requires use of the trigonometric parallax and which results in errors in diameter of around 10% — or that in the parallax if that is larger. The other method was to use Stefan's Law to derive diameter from the observed stellar luminosity at the Earth and the effective temperature. Here the largest uncertainty comes from that in T_{eff} which enters as the fourth power; the typical uncertainty in diameter is then 13%. These two determinations give values for diameter that agree very well — to typically 1.5%. Diameters are also given in Table 4.

Figure 13 shows diameter (determined from scaling factor) versus effective temperature with symbols indicating the metallicity implied by the energy distribution comparison. Metal–poor stars have a smaller diameter for a constant temperature. Open symbols are known multiple systems which would have larger diameters; typical error bars as well as larger individual errors are indicated. The dashed lines are structural model predictions from Baraffe et al. 1997, Chabrier & Baraffe 1997 (which use the NextGen atmospheres without the improved linelists) for an age of 10 Gyr. The models for 1 Gyr are not significantly different. The agreement is good except for known multiple systems and for LHS 1183 (a young flare star), LHS 135, LHS 2945, LHS 5327 and LHS 549 (an old variable star), which also seem to have too large a diameter. As far as we are aware none of these are known to be multiple, and LHS 549 has been searched for close companions using speckle by Leinert et al. 1997 with a negative result. These five stars merit further study for multiplicity.

7. Conclusions

We have obtained 1—2.5μm spectra for 42 disk and halo M1–M6.5 dwarfs. These data have been combined with new or published optical spectra, and energy distributions derived by flux calibrating and combining the individual spectral regions for each object. Bolometric luminosities have been determined and a relationship between bolometric magnitude and I−K color given.

The colors and energy distributions have been compared to synthetic photometry and spectroscopy generated by an upgraded version of the NextGen models, the AMES-Dusty models (Hauschildt, Allard & Baron 1999). These models use more recent TiO and H_2O linelists,

and include grain condensation and extinction. The agreement is much improved in the red region compared to earlier comparisons (e.g. Leggett et al. 1996). Problems remain with the match to the observed FeH features and also to the water bands. These problems are being addressed with ongoing work to calculate more complete linelists. Nevertheless we can determine effective temperatures for the sample to $\pm$100 K, metallicities to $\pm$0.25 dex, and radii to typically 10%. Recent structural models by Baraffe et al. 1997, Chabrier & Baraffe 1997 agree with the luminosities and radii derived except for five stars which may be previously unknown multiple systems: LHS 1183, LHS 135, LHS 2945, LHS 5327 and LHS 549.

We are very grateful to the staff at UKIRT, the University of Hawaii's 88–inch telescope, the Lowell Observatory and the Naval Observatory Flagstaff Station for their assistance in obtaining the data presented in this paper. UKIRT, the United Kingdom Infrared Telescope, is operated by the Joint Astronomy Centre Hilo Hawaii on behalf of the U.K. Particle Physics and Astronomy Research Council. FA acknowledges support from NASA LTSA NAG5-3435 and NASA EPSCoR grants to Wichita State University, and support from CNRS. PHH acknowledges partial support from the Pôle Scientifique de Modélisation Numérique at ENS-Lyon. This work was also supported in part by NSF grants AST-9417242, AST-9731450, and NASA grant NAG5-3505. Some of the calculations presented in this paper were performed on the IBM SP and the SGI Origin 2000 of the UGA UCNS and on the IBM SP of the San Diego Supercomputer Center (SDSC), with support from the National Science Foundation, on the Cray T3E of the NERSC with support from the DoE, and on the IBM SP2 of the French Centre National Universitaire Sud de Calcul (CNUSC) and the Cray T3E of the Commissariat a l'Energie Atomique (CEA). We thank all these institutions for a generous allocation of computer time.

REFERENCES

Allard, F., Hauschildt, P.H., Alexander, D.R., & Starrfield, S., 1997, ARA&A, 35, 137

Allard, F., Hauschildt, P.H. & Schwenke, D.W., 2000, ApJ, submitted

Baraffe, I., Chabrier, G., Allard, F. & Hauschildt, P. H., 1997, A&A, 327, 1054

Borysow, A., Jørgensen, U.G. & Zheng, C., 1997, A&A, 324, 185

Chabrier, G. and Baraffe, I., 1997, A&A, 327, 1039

Dawson, P.C. & de Robertis, M.M., 1998, AJ, 116, 2565

Delfosse, X. et al., 1997, A&A, 327, L25

Giclas, H.L., Burnham, R. & Thomas, N.G., 1971, Lowell Proper Motion Survey, The G Numbererd Stars (Flagstaff: Lowell Observatory)

Gizis, J.E., 1997, AJ, 113, 806

Gizis, J.E. & Reid, I.N., 1997, PASP, 109, 849

Gliese, W., & Jahreiss, H., 1991, Preliminary Version of the Third Catalog of Nearby Stars, Astronomisches Rechen–Institut Heidelberg Germany

Hauschildt, P.H., Allard F. & Baron, E., 1999, ApJ, 512, 377

Henry, T.J. Franz, O.G., Wasserman, L.H., Benedict, G.F; Shelus, P.J., Ianna, P.A., Kirkpatrick, J.D., McCarthy, D.W.Jr. 1999, ApJ, 512, 864

Henry, T.J, Kirkpatrick, J. D. & Simons, D. A., 1994, AJ, 108, 1437

Henry, T.J. & McCarthy Jr., D.W., 1993, AJ, 106, 773

Kirkpatrick, J. D., Henry, T. J., & Irwin, M.J., 1997, AJ, 113, 1421

Kirkpatrick, J. D., Henry, T. J., & McCarthy, D.W., 1991, ApJS, 77, 417

Kirkpatrick, J. D., Henry, T. J., & Simons, D. A., 1995, AJ, 109, 797

Leggett, S.K., 1992, ApJS, 82, 351 [L92]

Leggett, S.K., Allard, F., Berriman,G., Dahn, C.C. & Hauschildt, P.H., 1996, ApJS, 104, 117

Leggett, S.K., Allard, F., & Hauschildt, P.H., 1998, ApJ, 509, 836.

Leinert, C., Henry, T., Glindemann, A., & McCarthy D.W. Jr, 1997, A&A, 325, 159.

Luyten W.J. 1979, The LHS Catalogue, Second Edition (Minneapolis: University of Minnesota)

Metcalfe et al. 1966, ApJ, 456, 356

Monet, et al. 1992, AJ, 103, 638

Partridge, H. & Schwenke, D.W., 1997, J. Chem. Phys., 106, 4618

Reid, I.N., Hawley, S.L., & Gizis, J.E., 1995, AJ, 110, 1838

Ruiz, M.T. & Anguita, C., 1993, AJ, 105, 614

Schwenke, D. W., 1998 Chemistry and Physics of Molecules and Grains in Space. Faraday Discussions No. 109, 321. The Faraday Division of the Royal Society of Chemistry, London.

van Altena, W.F., Lee, J.T., & Hoffleit, E.D. 1994, The General Catalogue of Trigonometric Parallaxes (New Haven: Yale University Observatory)

Viti, S., Jones, H.R.A., Schweitzer, A., Allard, F., Hauschildt, P.H., Tennyson, J., Miller, S, Longmore, A.J., 1997, MNRAS, 291, 780

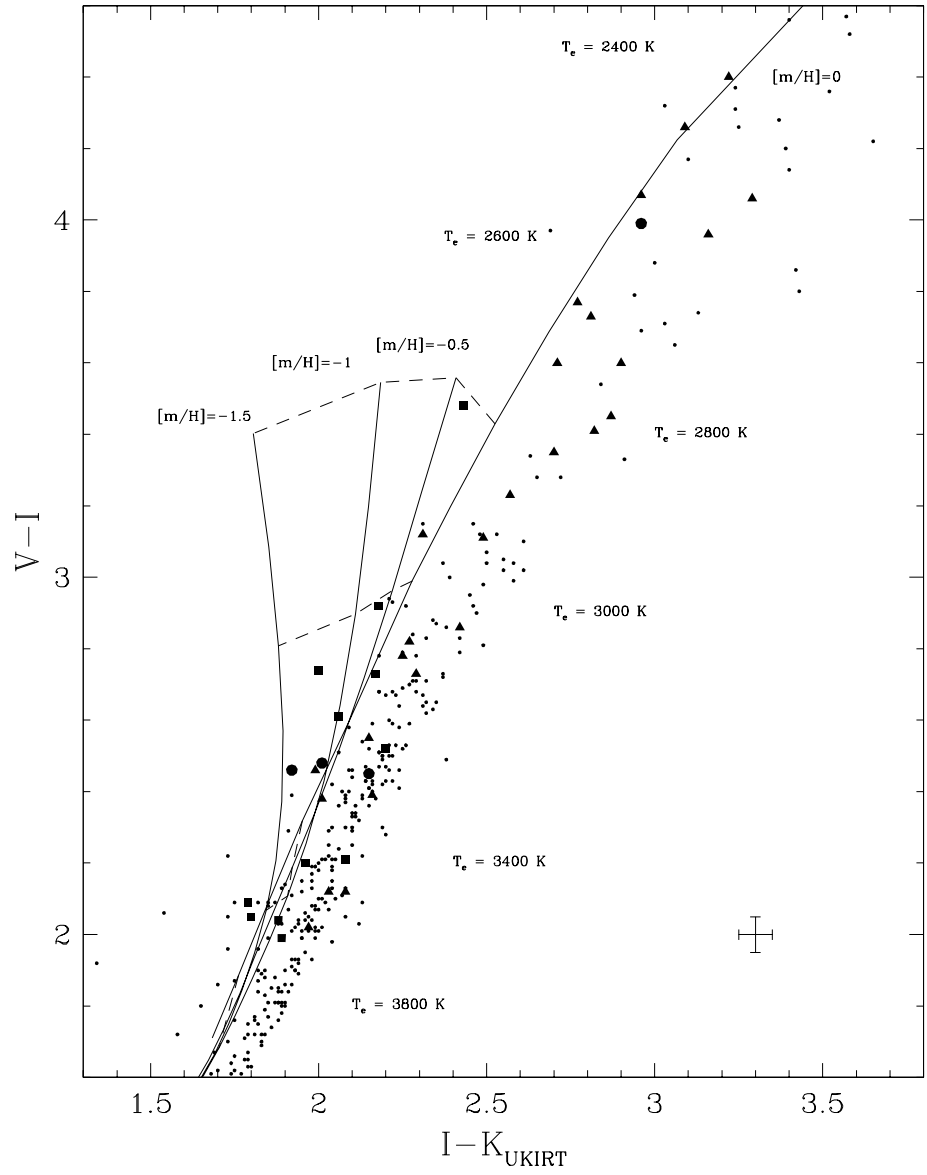

Fig. 1.— V−I:I−K diagram with model sequences for metallicities [m/H] = −1.5, −1, −0.5 and 0. Dashed lines connect fixed effective temperature values as indicated to the right. Filled symbols are this work, where symbol shapes represent kinematic populations: squares — halo, triangles — disk, circles — unknown. Dots are stars from Leggett et al. 1998 and from L92 (on the UKIRT JHK system).

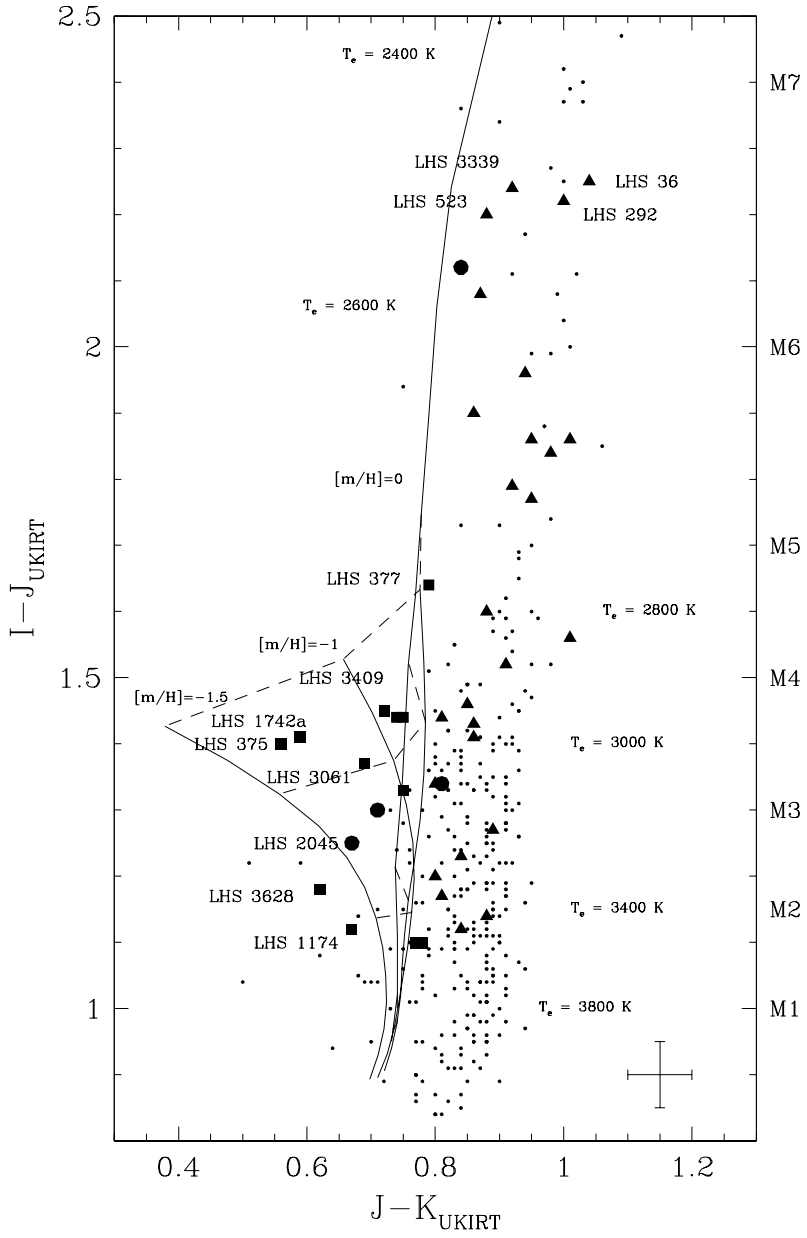

Fig. 2.— I−J:J−K diagram with model sequences using the same symbols as in Figure 1. Spectral types based on I−J (L92) are shown.

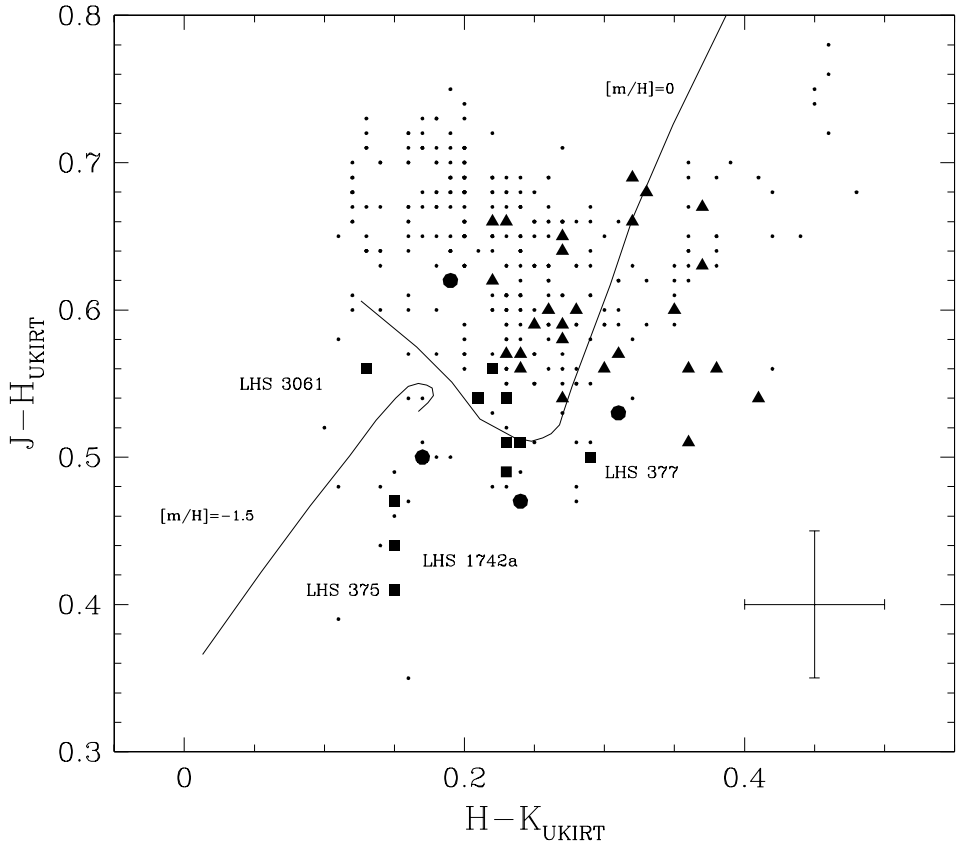

Fig. 3.— J−H:H−K diagram with model sequences using the same symbols as in Figure 1.

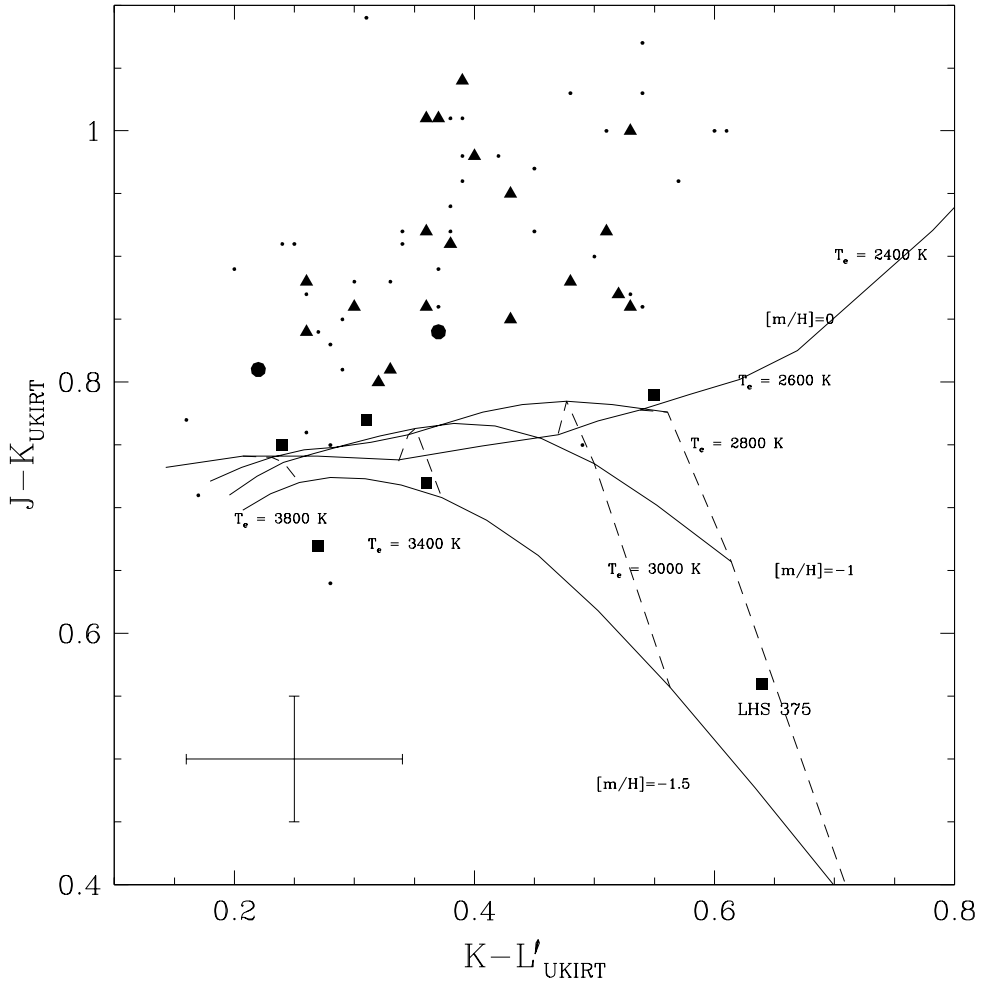

Fig. 4.— J−K:K−L′ diagram with model sequences using the same symbols as in Figure 1.

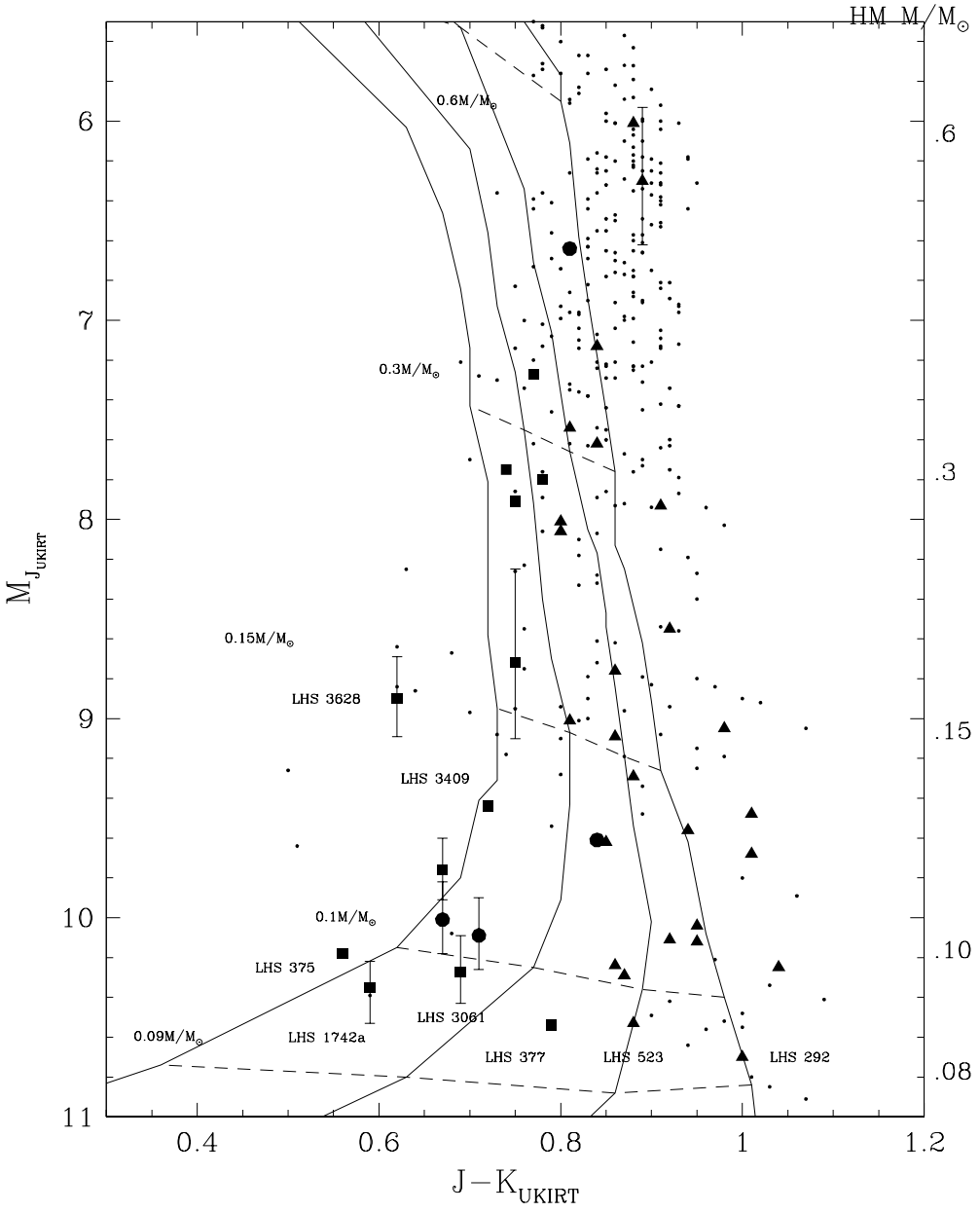

Fig. 5.— M_J:J−K with symbols as in Figure 1. Empirical masses for the disk stars from Henry & McCarthy 1993 are given on the right axis. Solid lines are isochrones from Baraffe et al. 1997, Chabrier & Baraffe 1997 for age 10 Gyr and metallicities from left to right: [m/H] $= -1.5, -1.0, -0.5, 0.0$. Dashed lines connect fixed mass values, as indicated.

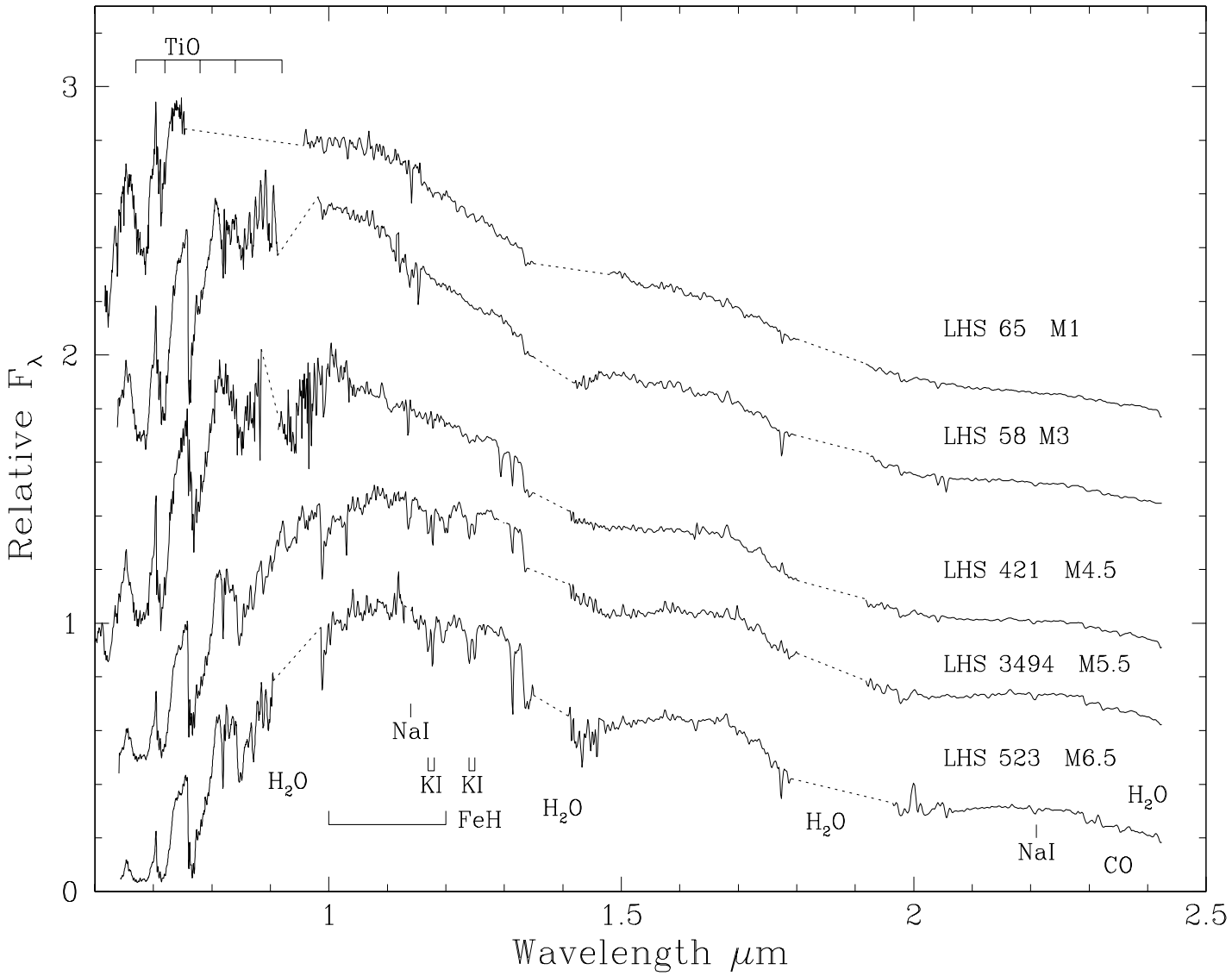

Fig. 6.— Spectral sequence for M dwarfs where the spectra have been normalised to the flux at 1.2μm and offset.

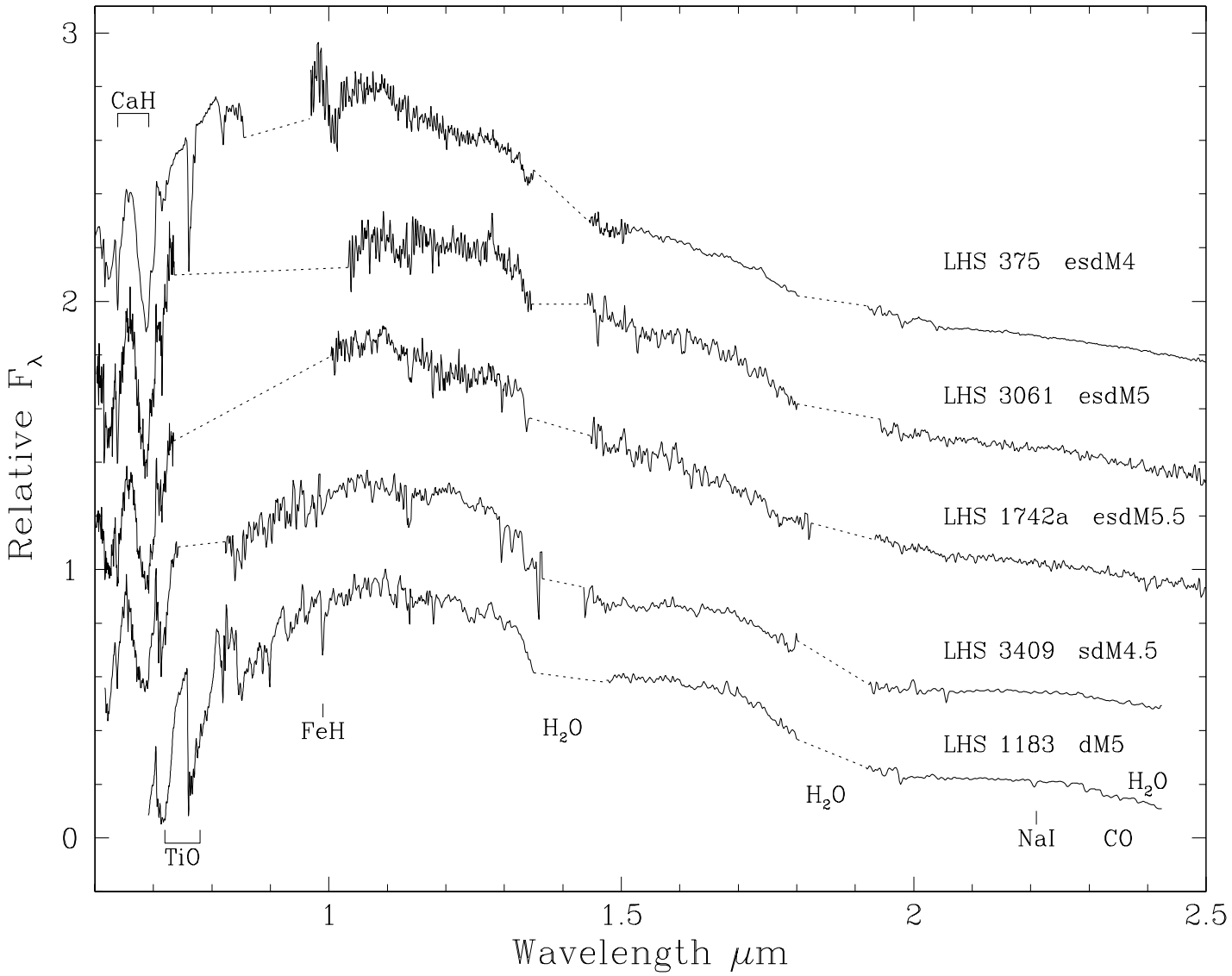

Fig. 7.— Spectral sequence for subdwarfs where the spectra have been normalised to the flux at 1.2μm and offset.

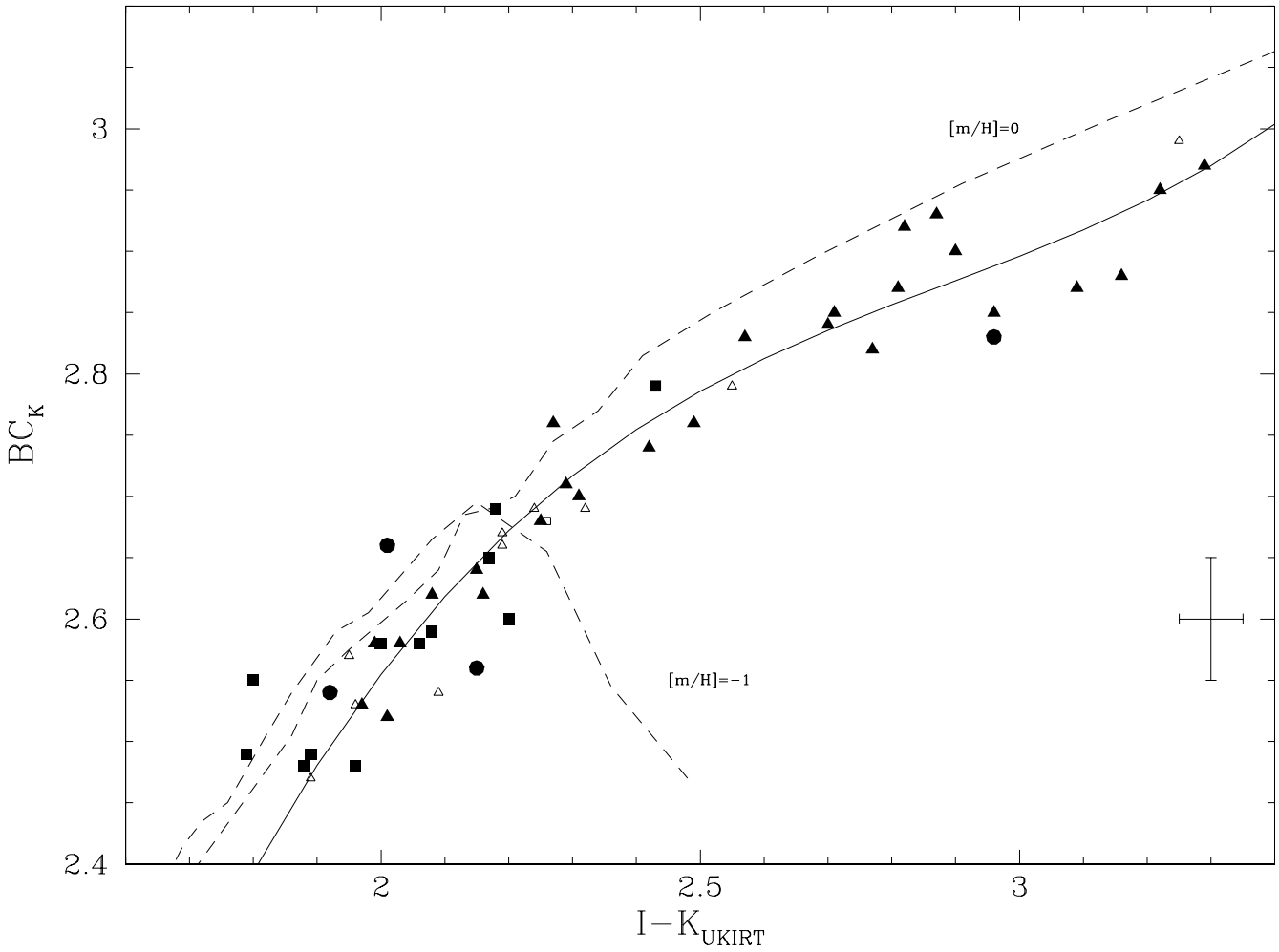

Fig. 8.— Bolometric correction at K versus I−K. Filled symbols are this work, open are from Leggett et al. 1996. Symbol shape represent kinematic populations: squares — halo, triangles — disk, circles — unknown. Model sequences for [m/H]=0 and [m/H]= −1 are overlaid as dashed lines. The solid line is the empirical fit to the disk stars.

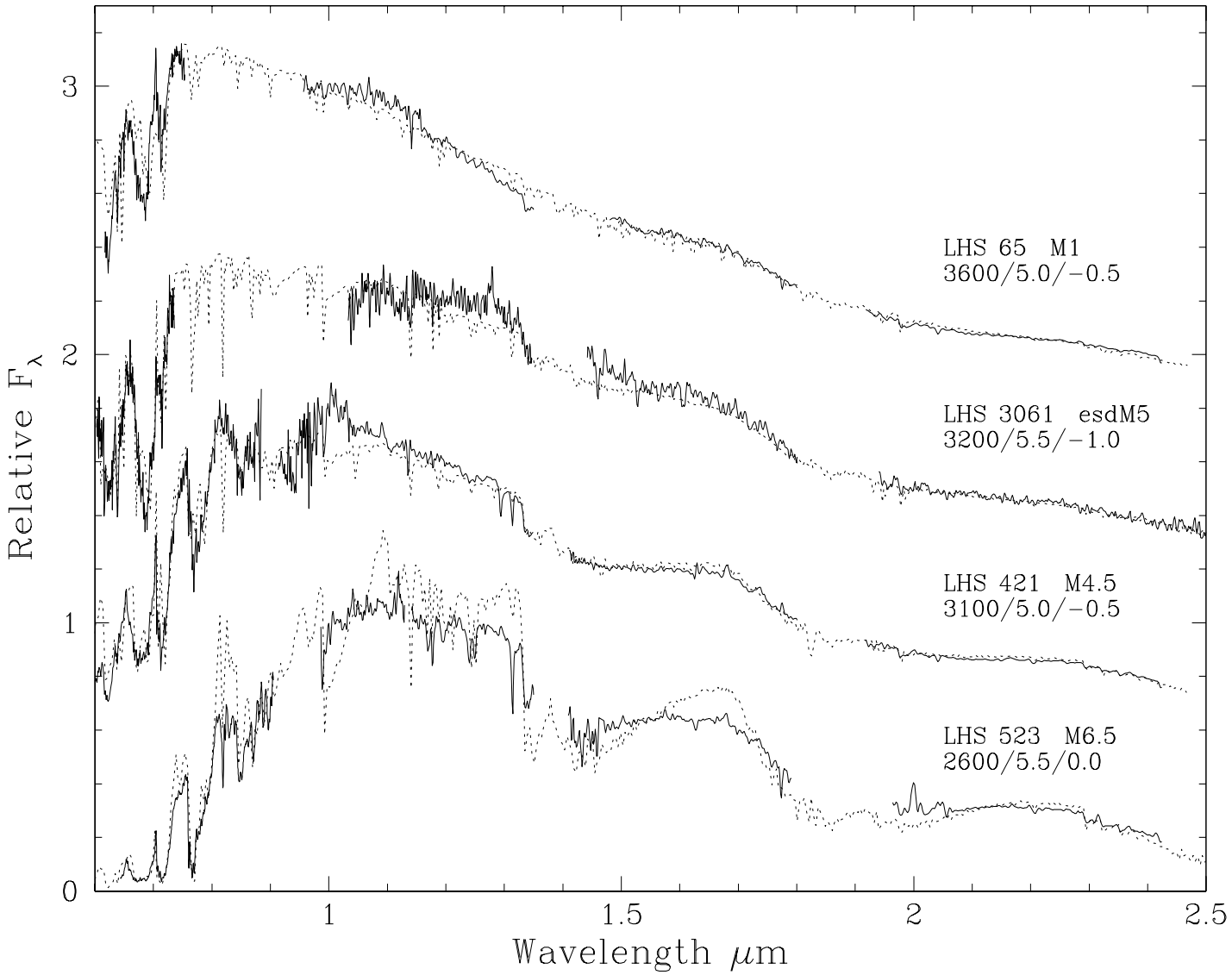

Fig. 9.— Comparison of synthetic (dashed line) and observed (solid line) spectral energy distributions, where the spectra have been normalised to the flux at 1.2μm and offset. The best fit model parameters T_{eff}/log g/[m/H] are given for each star.

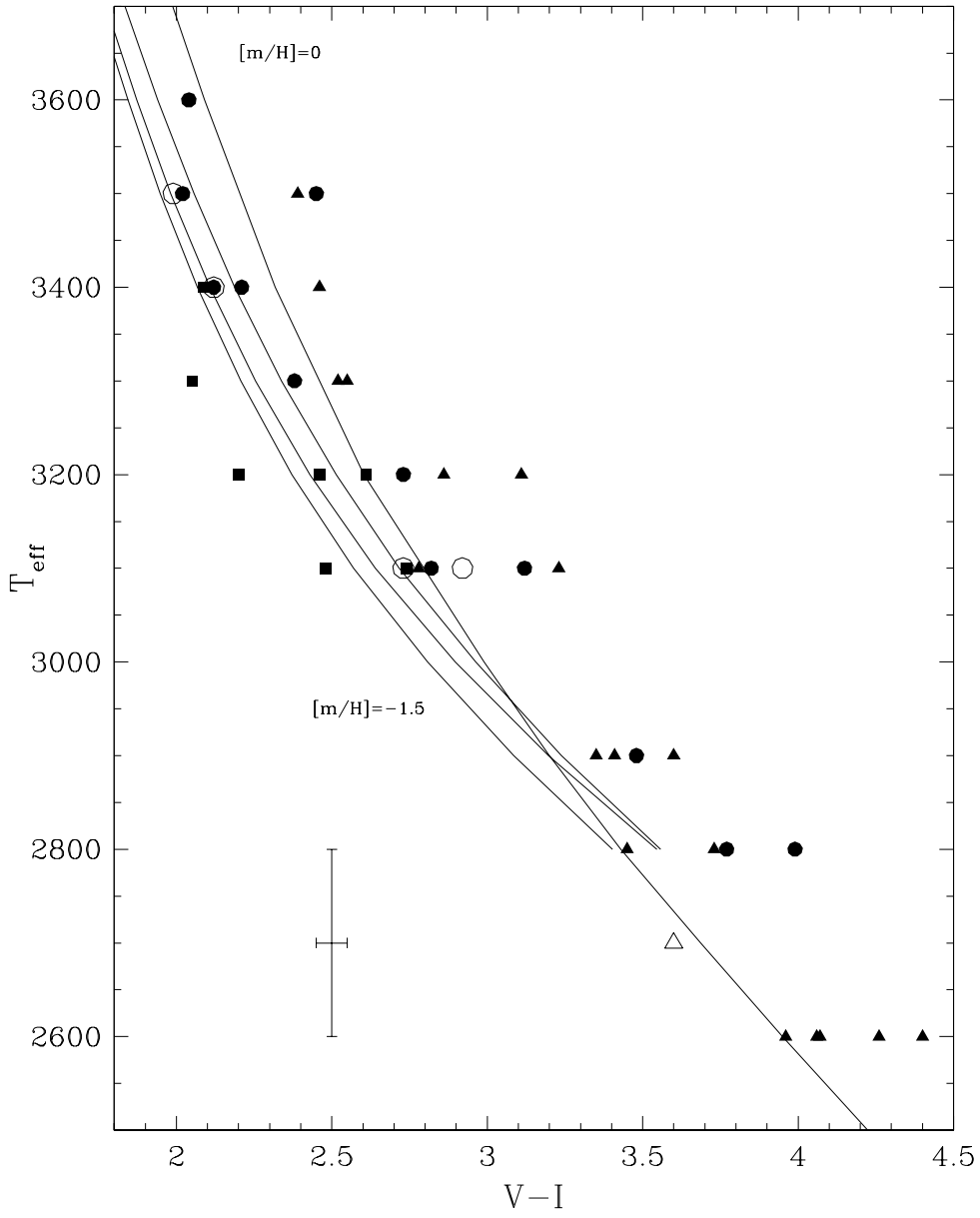

Fig. 10.— T_{eff} as a function of V−I. Symbols indicate the metallicity implied by the energy distribution: squares — [m/H]= −1.0, circles — [m/H]= −0.5, triangles — [m/H]=0. Open symbols are multiple systems. Model sequences for [m/H]=0, = −0.5, = −1.0 and = −1.5 are also shown where for hotter stars decreasing metallicity at a constant temperature results in bluer V−I.

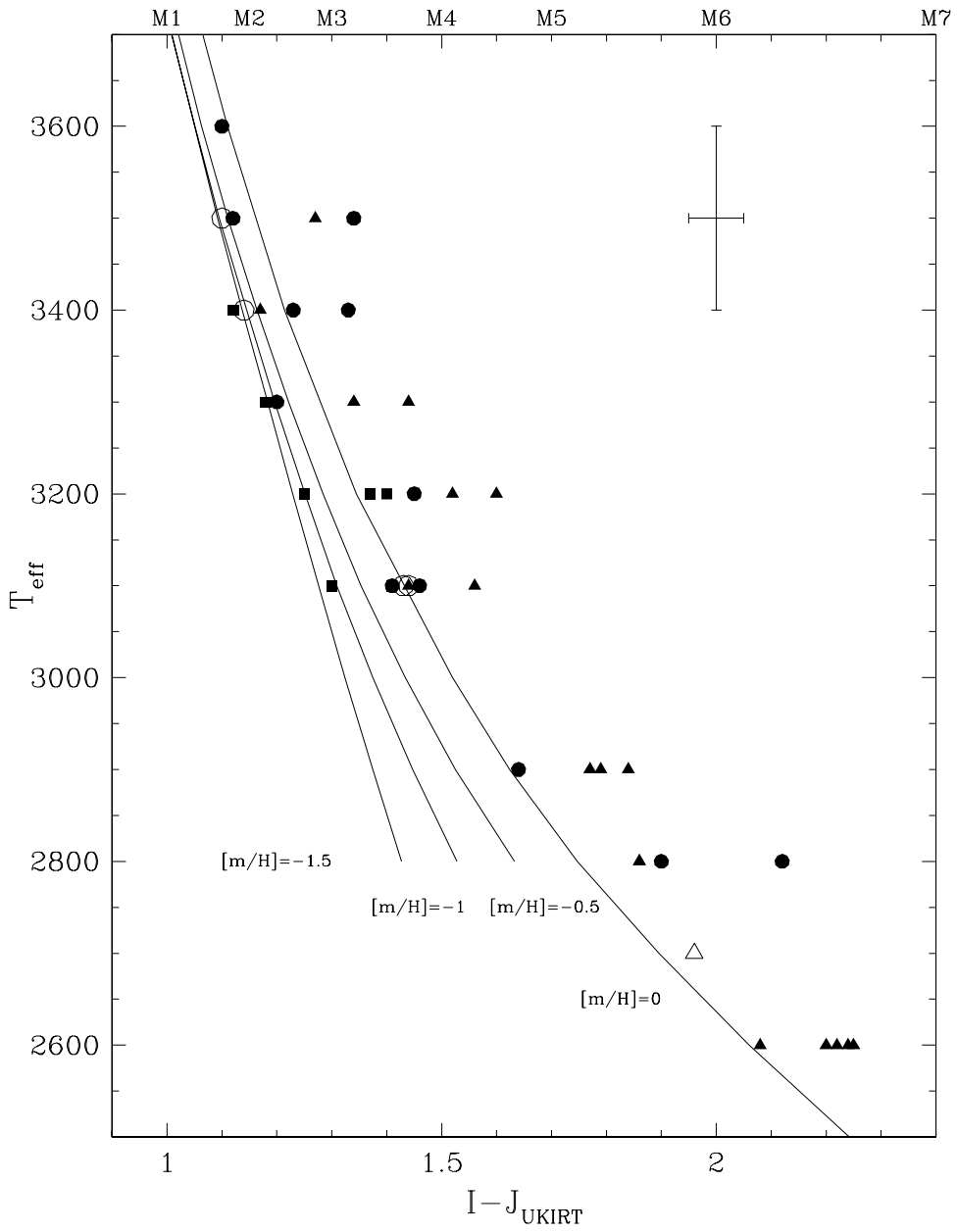

Fig. 11.— T_{eff} as a function of I−J. Symbols are as in Figure 10.

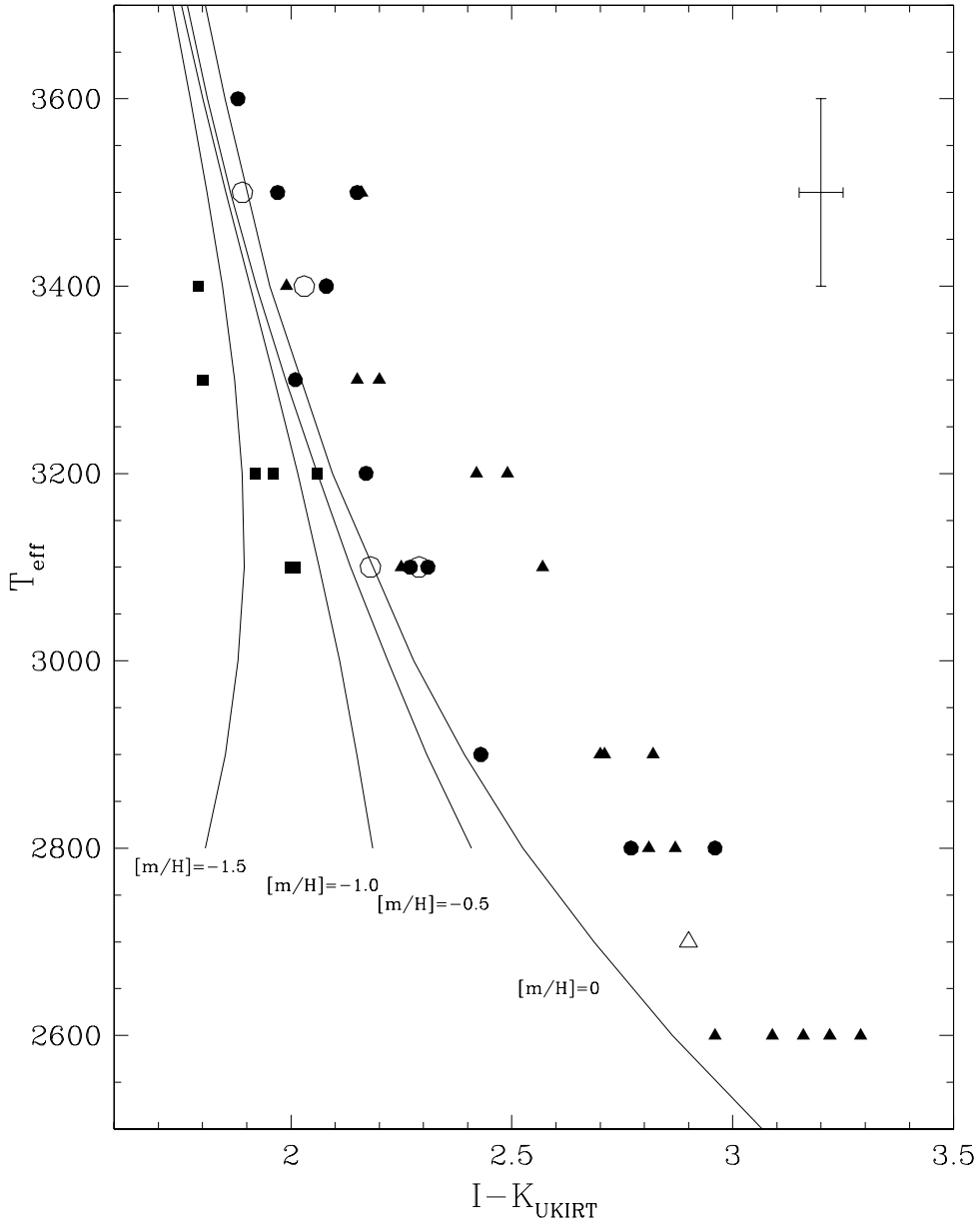

Fig. 12.— T_{eff} as a function of I−J. Symbols are as in Figure 10.

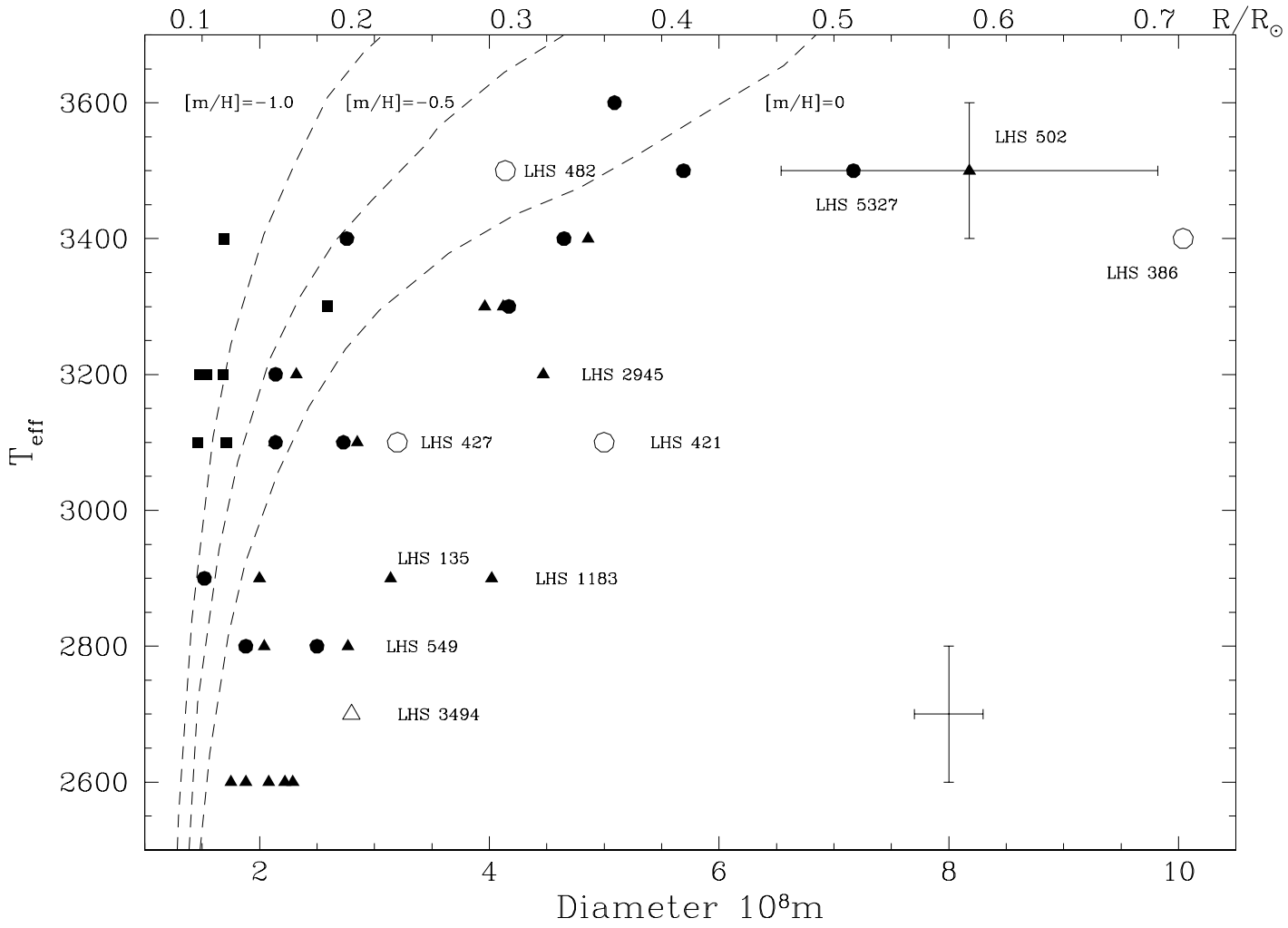

Fig. 13.— Diameter (derived by scaling) as a function of T_{eff}. Symbols are as in Figure 10 and dashed lines are structural model calculations from Baraffe et al. 1997, Chabrier & Baraffe 1997. Stars with apparently large diameters are identified, as is a star with a large uncertainty due to parallax error.